Charged Chiral Derivatization for Enantioselective Imaging of D-, L-2-hydroxyglutaric acid Using Ion Mobility Spectrometry/Mass Spectrometry†

Eiji Sugiyama, [a] Yuki Nishiya,[a] Kenji Yamashita,[a] Ryo Hirokawa,[a] Yoshiteru Iinuma,[b] Takashi Nirasawa,[c] Hajime Mizuno,[a, d] Yoshitaka Hamashima[a] and Kenichiro Todoroki*[a]

A newly synthesized charged chiral tag enabled enantioselective imaging of D-, L-2-hydroxyglutaric acid, which are independently associated with the regulation of DNA methylation. The tag-conjugated diastereomers were ionized efficiently through MALDI, separated by ion mobility spectrometry, and further separated from other molecules in mass spectrometry. On-tissue chiral derivatization using the tag facilitated the visualization of different distributions of the two isomers in the mouse testis.

Physiologically active substances are mostly chiral, and their enantiomers exhibit different biological properties. Various techniques, typically involving gas chromatography, liquid chromatography (LC), or electrophoresis have been developed to detect minor enantiomers in biological specimens[1-3]. These methods have significantly contributed to our understanding of biological and clinical phenomena, including the correlation between disease progression and the concentration of minor enantiomers[4, 5].

Distribution analysis of chiral small molecules in a biological specimen is challenging. Although autoradiography (ARG) and immunohistochemistry (IHC) have provided important spatial information for some minor chiral amino acids[6-8], these methods have certain limitations. For instance, ARG cannot be used for the analysis of endogenous molecules since it requires the exogenous administration of radioisotope-labelled compounds. IHC requires careful optimization as it requires tissue fixation, in which small molecules can be dislocated. Therefore, there is a need for an alternative method to analyse the distribution of a range of endogenous chiral molecules.

Ion mobility spectrometry/mass spectrometry (IMS/MS) has emerged as the alternative method for enantioselective imaging. IMS/MS is capable of separating ionized molecules in a gas phase in less than one second, and recent reports have demonstrated the advantageous use of IMS/MS in high-throughput bioanalysis of chiral amino acids[9-10]. However, the most recent study using chiral derivatization for amino acids did not succeed in imaging due to insufficient signal intensities of the target ions ($[M - H + 2Na]^+$) [11]. Therefore, enantioselective imaging through IMS/MS remained an unattained goal as of yet.

D- and L-2-hydroxyglutaric acid (D-, L-2HG) are each associated with different types of cancers and metabolic disorders[12]. Since the two enantiomers exist as endogenous metabolites and their levels are independently regulated, discriminating between the two is important for precise diagnosis or pathological studies[13]. We previously found an enantioseparation method for D-, L-2HG in IMS [14]. In the method, D-, L-2HG were separated as $[M + H]^+$ of diastereomeric derivatives obtained with (*S*)-1-(4,6-dimethoxy-1,3,5-triazin-2-yl)pyrrolidin-3-amine (DMT(*S*)A). However, similar to the aforementioned study, preliminary experiments towards imaging did not provide successful results due to insufficient signal intensity. In MS imaging, detection of analyte in $[M]^+$ is known to provide successful results[15-17]. Therefore, structural modification of DMT(*S*)A to a permanently charged compound was expected to be the key approach to achieving enantioselective imaging.

In this study, based on a high stability and ionization efficacy of tris(2,4,6-trimethoxyphenyl)carbenium derivatives[18], we designed (*S*)-1-(4-(bis(2,4,6-trimethoxyphenyl)methyliumyl)-3,5-dimethoxyphenyl)pyrrolidine-3-amine (BTMD(*S*)A) as a cationic chiral derivatization reagent (Fig. 1A). BTMD(*S*)A was synthesized by a reaction of tris(2,4,6-trimethoxyphenyl)carbenium tetrafluoroborate with (*S*)-3-(Boc-amino)-1-(4-(bis(2,4,6-trimethoxyphenyl)methyliumyl)-3,5-

[a] *School of Pharmaceutical Sciences, University of Shizuoka, 52-1 Yada, Suruga-ku, Shizuoka, 422-8526, Japan.*
[b] *Okinawa Institute of Science and Technology Graduate University, 1919-1 Tancha, Onna-son, Kunigami-gun, Okinawa, Japan 904-0495.*
[c] *Daltonics division, Bruker Japan K.K., Moriyacho Kanagawa-ku, Yokohama-shi, Kanagawa, Japan 221-0022*
[d] *Laboratory of Analytical Chemistry, Faculty of Pharmacy, Meijo University, 150 Yagotoyama, Tempaku, Nagoya, 468-8503, Japan*
*. Corresponding author
†Electronic Supplementary Information (ESI) available: experimental methods, supplemental figures, spectroscopic data.

dimethoxyphenyl)pyrrolidine, followed by deprotection of the Boc (ESI, Fig. S1). The successful synthesis of BTMD(*S*)A was confirmed by a combination of nuclear magnetic resonance (NMR) measurement (^{1}H) and MALDI/MS (ESI, Fig. S2, S3).

BTMD(*S*)A derivatives of D-, L-2HG were separated with a two-peak resolution (*R*s) over 1.8 in IMS (Fig. 1B). When 1-(3-dimethylaminopropyl)-3-ethylcarbodiimide (EDC) and 3*H*-1,2,3-triazolo[4,5-b]pyridine-3-ol (HOAt) were used as condensation reagents, isomerization of the enantiomers was not observed. In contrast, the use of triphenylphosphine and 2,2'-dipyridyl disulphides caused significant isomerization during the derivatization (Fig. S4). By using EDC and HOAt, localization of D-, L-2HG in dried droplets, prepared with the reaction mixtures of D-, L-, and DL-2HG (racemate), was successfully visualized (Fig. 1C).

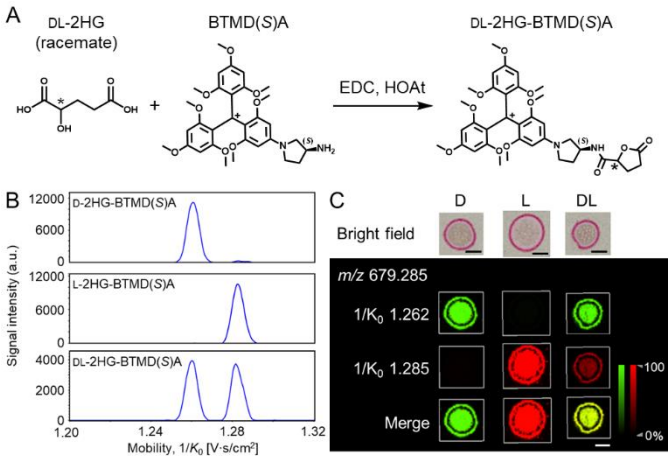

Fig. 1. Separation and imaging of D-, L-2HG using BTMD(*S*)A and IMS/MS. A: Scheme of diastereomeric derivatization of D-, L-2HG using BTMD(S)A. B: Mobilogram of BTMD(*S*)A derivatives of D-2HG (upper), L-2HG (middle), and DL-2HG (racemate, lower). C: Visualization of localized the BTMD(*S*)A derivatives. Upper: optical image; Lower: Ion images of BTMD(*S*)A-D-2HG (green) and BTMD(*S*)A-L-2HG (red). Scale bar = 1 mm.

To evaluate the signal intensity obtained from BTMD(*S*)A derivatives, DMT(*S*)A derivatives were used as the control (Fig. 2A). DL-2HG (racemate) was reacted with BTMD(*S*)A or DMT(*S*)A, and the reaction mixtures were spotted and dried on a conductive slide glass or the slices of mouse testis. The dried droplets were uniformly coated by a matrix (2,5-dihydroxybenzoic acid, DHB) using an automatic sprayer (Fig. 2B). Averaged signal intensities obtained from the spot area was obviously higher in BTMD(*S*)A derivatives as compared to those of DMT(*S*)A derivatives (> 10 times for the droplets on glass, > 100 times for those on mouse testis) (Fig. 2B, 2C, S5). In addition, the effect of ion suppression by testis components for the BTMD(*S*)A derivatives was smaller (38%) as compared to that for the DMT(*S*)A derivatives (94%) (Fig. 2C). These results supported that BTMD(*S*)A is better suitable for the imaging of D-, L-2HG.

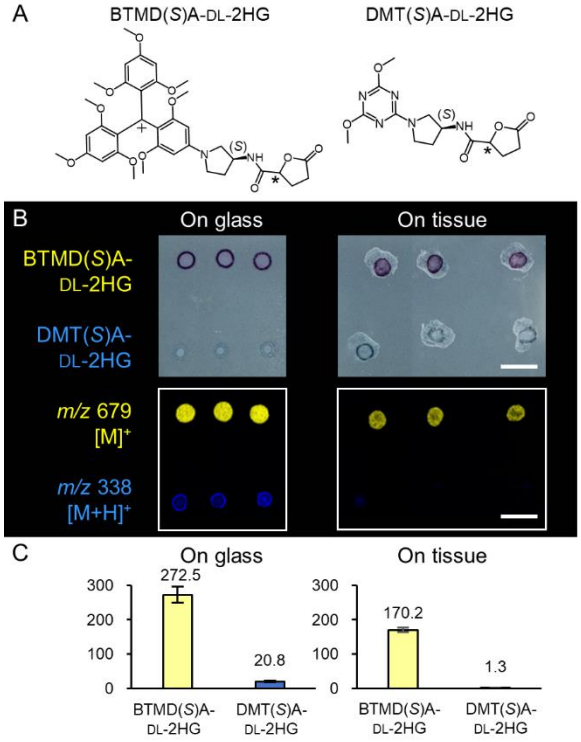

Fig. 2: Comparison of the signal intensities in MALDI/MS between the DL-2HG derivatives using BTMD(*S*)A and DMT(*S*)A. A: Chemical structure of the diastereomers. B: Bright and Ion images of the measured samples. Reaction mixtures after derivatization were spotted and dried on the ITO-coated glass (left) or the slices of mouse testis (right). The images were obtained after the coating with DHB. Ion images of the BTMD(*S*)A-DL-2HG and DMT(*S*)A-DL-2HG are shown in yellow and blue, respectively. C: Mean intensities of the DL-2HG derivatives. The data are shown as mean ± S.D. (n = 3). Scale bar = 5 mm.

To confirm that the BTMD(*S*)A derivatization can proceed in tissues, we prepared a series of dried droplets on the mouse testis. Solutions of a stable isotope-labelled 2HG ($^{13}C_5$-DL-2HG in 0, 10, 100, 1000 µM) was used to exclude the influence of the signals from endogenous D-, L-2-HG. After spraying a mixture of BTMD(*S*)A, EDC, and HOAt on the dried droplets of $^{13}C_5$-DL-2HG, the samples were incubated at 25°C for 2 h in a glass dish containing a paper sheet wet with a 90% acetonitrile aqueous solution. The slices were coated by DHB. BTMD(*S*)A derivatives of D-, L-$^{13}C_5$-2HG were able to be detected, and the relative mean intensity were about 1, 1300, 1900, 4500 for the spots containing 0, 5, 50, 500 pmol/spots of each enantiomer (Fig. S6). The concentration-dependent signal increase supported the feasibility of on-tissue chiral derivatization for visualizing endogenous D-, L-2-HG on the mouse testis.

To visualize the distribution of endogenous D-, L-2HG, the mixture of BTMD(*S*)A, EDC, and HOAt was sprayed to the slices of mouse testis. After the incubation and the coating in the same way described above, measurement using MALDI/IMS/MS and a following H&E staining were performed. Consistently with the result of a previous report using LC/MS[19],

averaged signal intensity of L-2HG was obviously higher than that of D-2HG (Fig. 3A). Furthermore, different distributions of the two enantiomers were able to be observed. The L-2HG levels were different between the seminiferous tubules (Fig. 3B), indicating a possibility of the change associated with sperm maturation.

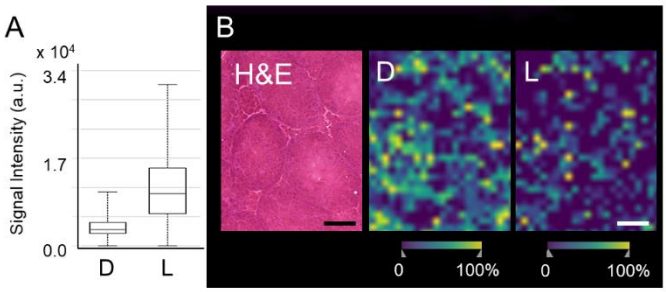

Fig. 3: Detection and visualization of endogenous D-, L-2HG in the mouse testis using BTMD(*S*)A and MALDI/IMS/MS. A: Signal intensity of the D-, L-2HG-BTMD(*S*)A obtained from the measured area. B: Bright image of the mouse testis section after H&E staining (left) and the ion images of D-, L-2HG (right). Scale bar = 100 µm.

In conclusion, BTMD(*S*)A enabled enantioselective imaging of D-, L-2HG in dried droplets and the mouse testis through the formation of the diastereomers and MALDI/IMS/MS analysis. The carbenium and (*S*)-pyrrolidine-3-amine structure in BTMD(*S*)A provided the high ionization efficacy in MALDI and sufficient resolution in IMS. The on-tissue chiral derivatization was capable for visualizing the different distribution D-, L-2HG in the mouse testis. These results demonstrated that a cationic chiral tag designed for separation in IMS would be a useful tool for enantioselective imaging of chiral small molecules. Future development of similar tags can be expected to enable enantioselective imaging of various chiral molecules.

Author Contributions are as follows. **E.S.**: Conceptualization, Data curation, Formal Analysis, Resources, Funding acquisition, Investigation, Methodology, Project administration, Resources, Visualization, Writing - Original draft preparation, Writing – review & editing. **Y.N.**: Data curation, Formal Analysis, Methodology, Visualization. **K.Y**.: Data curation, Methodology, Resources, Writing – review & editing. **R.H.**: Data curation, Methodology. **Y.I.**: Data curation, Methodology, Resources, Writing – review & editing. **T.N.**: Data curation, Resources. **H.M.**: Methodology, Resources, Funding acquisition, Writing – review & editing. **Y.H.**: Methodology, Resources, Writing – review & editing, Supervision. **K.T.**: Methodology, Resources, Writing - Reviewing and Editing, Supervision, Funding acquisition.

This work was supported by JSPS KAKENHI (grant numbers 20K15972 and 22K15264) and the research foundation for pharmaceutical sciences to E.S.

Conflicts of interest

There are no conflicts to declare.

References

1 J. Byron, J. Kreuzwieser, G. Purser, J. van Haren, S. N. Ladd, L. K. Meredith, C. Werner and J. Williams, *Nature*, 2022, **609**, 307-312.
2 E. Sugiyama, M. Nakamura, H. Mizuno, A. Furusho and K. Todoroki, *Anal. Sci.*, 2023, **39**, 463-472.
3 M. Svidrnoch, A. Pribylka, V. Bekarek, J. Sevcik, V. Smolka and V. Maier, *J. Chromatogr. A*, 2016, **1467**, 383-390.
4 M. Numako, T. Takayama, I. Noge, Y. Kitagawa, K. Todoroki, H. Mizuno, J. Z. Min and T. Toyo'oka, *Anal. Chem.*, 2016, **88**, 635-639.
5 A. Furusho, R. Koga, T. Akita, M. Mita, T. Kimura and K. Hamase, *Anal. Chem.*, 2019, **91**, 11569-11575.
6 K. Imai, T. Fukushima, T. Santa, H. Homma, J. Sugihara, H. Kodama and M. Yoshikawa, *Proc. Jpn. Acad., Ser. B*, 1997, **73**, 48-52.
7 J. M. Wong, O. O. Folorunso, E. V. Barragan, C. Berciu, T. L. Harvey, J. T. Coyle, D. T. Balu and J. A. Gray, *J. Neurosci.*, 2020, **40**, 9564-9575.
8 S. M. Williams, C. M. Diaz, L. T. Macnab, R. K. Sullivan and D. V. Pow, *Glia*, 2006, **53**, 401-411.
9 J. M. Will, A. Behrens, M. Macke, C. D. Quarles, Jr. and U. Karst, *Anal. Chem.*, 2021, **93**, 878-885.
10 Y. Li, B. Zhou, K. Wang, J. Zhang, W. Sun, L. Zhang and Y. Guo, *Anal. Chem.*, 2021, **93**, 13589-13596.
11 C. Xie, Y. Chen, X. Wang, Y. Song, Y. Shen, X. Diao, L. Zhu, J. Wang and Z. Cai, *Chem. Sci.*, 2022, **13**, 14114-14123.
12 D. Ye, K. L. Guan and Y. Xiong, *Trends Cancer*, 2018, **4**, 151-165.
13 J. Kalinina, J. Ahn, N. S. Devi, L. Wang, Y. Li, J. J. Olson, M. Glantz, T. Smith, E. L. Kim, A. Giese, R. L. Jensen, C. C. Chen, B. S. Carter, H. Mao, M. He and E. G. Van Meir, *Clin. Cancer Res.*, 2016, **22**, 6256-6265.
14 S. Fukui, E. Sugiyama, H. Mizuno, I. Sakane, D. Asakawa, K. Saikusa, Y. Nishiya, Y. Amano, K. Takahara, D. Higo, T. Toyo'oka and K. Todoroki, *J. Sep. Sci.*, 2021, **44**, 3489-3496.
15 Z. Ma, J. Yuan, J. Xu, L. Li, C. Tang, L. Chang, R. J. Quinn, L. Qin, J. Liu and Y. Ye, *Anal. Chem.*, 2022, **94**, 14917-14924.
16 E. Sugiyama, M. M. Guerrini, K. Honda, Y. Hattori, M. Abe, P. Kallback, P. E. Andren, K. F. Tanaka, M. Setou, S. Fagarasan, M. Suematsu and Y. Sugiura, *iScience*, 2019, **20**, 359-372.
17 I. Kaya, S. M. Brulls, J. Dunevall, E. Jennische, S. Lange, J. Martensson, A. G. Ewing, P. Malmberg and J. S. Fletcher, *Anal. Chem.*, 2018, **90**, 13580-13590.
18 C. Denekamp, J. Lacour, B. Laleu and E. Rabkin, *J. Mass Spectrom.*, 2008, **43**, 623-627.
19 X. Teng, M. J. Emmett, M. A. Lazar, E. Goldberg, J. D. Rabinowitz, *ACS Chem. Biol.*, 2016, **11**, 2420-2427.